

High Speed Chemical Vapor Communication Using Photoionization Detectors

Mustafa Ozmen, Eamonn Kennedy, Jacob Rose, Pratistha Shakya, Jacob K. Rosenstein, and Christopher Rose
School of Engineering

Brown University, Providence, RI

Email: mustafa_ozmen, eamonn_kennedy, jacob_rose1, pratistha_shakya, jacob_rostein, christopher_rose@brown.edu

Abstract—We consider data transfer between a chemical vapor emitter and photoionization detectors (PIDs) under constant velocity gas flow in a constrained environment (flow tube). We show that the system, though stochastic owing to flow unsteadiness, is (on average) linear and then characterize the channel using a Karhunen-Loeve (KL) expansion. We measure bit error rates using straightforward detection methods in the KL-produced signal space. Data rates of 20 bps are easily achieved at $\approx 10^{-3}$ error rate and we suspect that similarly low error rates are achievable at much higher bit rates using suitable adaptive equalization methods.

Index Terms—Molecular Communication, Chemical Communication, Gas Flow Channel

I. INTRODUCTION

Communication using chemicals in a gas flow [1] is an active area of research owing to its potential utility in environments hostile to electromagnetic or acoustic radiation. Since the first demonstration of molecular communication [1], a number of researchers have studied chemical communication between emitters and sensors in different environments. Some studies have been theoretical, seeking upper and lower bounds for the capacity of molecular communication channels [2]–[4] and recently nonlinear techniques have been applied to improve data rates [5]. Nonetheless, bit rates for molecular communication in a constrained but generally turbulent environment much above a bit per second (bps) at low error rates have remained elusive.

Here we consider a refined version of the exquisitely simple [6] experiment wherein chemical vapor (isopropanol) is released into steady airflow and sensed downstream. Here vapor is “puffed” through a tube and sensed using photoionization detectors (PIDs) as shown in FIGURE 1. Without characterizing the airflow in the tube – which we know through separate smoke tracer experiments is unsteady/turbulent – we will show that using relatively simple modulation and detection methods allows data rates of 20 bps at an error rate of approximately 10^{-3} . Furthermore, we suspect similarly good performance can be achieved at much higher bit rates by employing adaptive equalization methods.

II. EXPERIMENTAL SYSTEM

An experimental demonstration system was constructed to explore high-speed chemical vapor detection and signaling [7]. As illustrated in FIGURE 1, a solenoid valve controls the release of solvent vapors into an enclosed flow tube, where they are carried by a background airflow towards several photoionization detectors (200B miniPID, Aurora Scientific). The bulk airflow is controlled by two fans, while the transmitted vapor flow rate is regulated by a variable-area flowmeter. For the data presented here, the bulk air velocity is $v \approx 4$ m/s, the distance between the transmitter

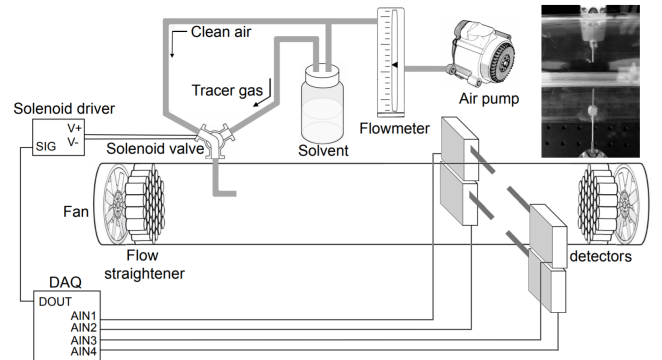


Fig. 1. Diagram of the benchtop experimental setup. The total tube length was 3.3 m. Sensor inlets could be placed at varying distance from the solenoid valve input with orientations either normal or orthogonal to the flow-line. In the configuration shown, all 4 PID sensors are located at $D = 0.8$ m and directed orthogonal to the flow-line (inset photograph, 2 sensors incident into the flow tube). Wind speed was adjusted by computer control of the two parallel-flowing fans. This configuration is a modification of a previous reported setup [7].

and detectors is 1.4 meters, and the diameter of the flow tube is 0.07 meters (so the path aspect ratio is 20:1).

III. THE CHANNEL

A sequence of brief (with duty cycle much less than the pulse period) vapor pulses are released (logical 1) or not (logical 0) into the flow tube. If we denote the time course of emitted vapor as $x[n]$, the system produces output $y[n]$ in response as

$$y[n] = S\{x[n]\} + w[n] \quad (1)$$

where $S\{\}$ summarizes the effect of fluid transport on a chemical released into the system with concentration time course $x[n]$, and $w[n]$ is the noise process added at the downstream sensor (receiver).

A. Linear or Nonlinear?

Fluid flow can be highly nonlinear, and nonlinearity introduces sometimes difficult analytic complications. For instance, there is no requirement for continuity and even slight variations ϵ in the input could yield dramatically different outputs under arbitrary distance measures $d[S\{x_1[n]\}, S\{x_1[n] + \epsilon z[n]\}]$ where ϵ is sufficiently small that $|\epsilon z[n]| \ll 1$. And even in cases where small input deviations yield similar outputs, nonlinearity implies that if $y_1[n]$ corresponds to input $x_1[n]$ and $y_2[n]$ corresponds to input $x_2[n]$, $S\{\}$ will NOT in general obey superposition. The implication for effective communication is that a map between all

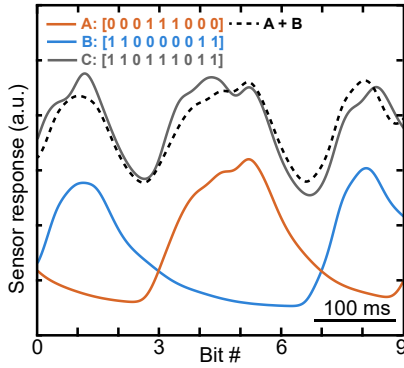


Fig. 2. Three input bit patterns, A (orange line), B (blue line) and C (gray line) which satisfy $A + B = C$ and their corresponding responses are shown. The extent of linearity can be visually assessed by the comparison of the C response with the superposition of the responses to its component patterns $A + B$ (dotted black line).

input sequences and their corresponding output sequences must be constructed. The virtual impossibility of such a task (absent severely circumscribed inputs) is the reason why we often seek a small deviations approximation to a nonlinear system about "operating points" where we can assume the system behaves almost linearly. So, it was important to investigate the linearity/nonlinearity of our system.

As depicted in FIGURE 1, a chemical is injected into a flow and detected by sensors downstream. We note that while the flow solutions can be nonlinear, unless the *chemical itself* – not the injection process – affects flow, then *the system is always linear*, although certainly time-varying, owing to factors like wind speed variation. Put another way, if the chemical injection process itself changes the air flow, then the air flow patterns will be dependent on chemical injection, regardless of downstream concentration profiles, and thus potentially provoke nonlinear response. Alternatively, if the chemical is simply "along for the ride" it presence/absence would not affect flow.¹

We tested system linearity by noting that if emission *does* affect the flow pattern, we would not expect (owing to nonlinearity of the underlying Navier-Stokes equations) a superposition of different temporal emission concentration patterns to result in a superposition of the respective concentration patterns. This hypothesis is explored in FIGURE 2 where the average responses to two input bit sequences A and B were recorded separately and then the average response to input $C = A + B$ was recorded. We see that $S(A) + S(B) \approx S(A + B)$. In fact, the difference between the cumulative pattern $S(A + B)$ and the sum of its components is comparable. This result suggests our system is roughly linear.

B. Linear But Stochastic: a Karhunen-Loeve approach

Since we can reasonably assume $S\{\}$ linear, we can express $y[n]$ as

$$y[n] = \sum_k x[k]h[n-k] + w[n] \quad (2)$$

¹We ignore "butterfly effects" through which the behavior of strongly chaotic systems can diverge dramatically even with infinitesimally small input variations. That is, we will assume that chemical presence/absence does not affect the properties of the carrier fluid over time scales of interest.

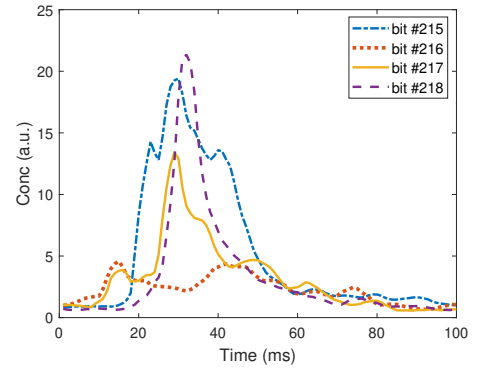


Fig. 3. Concentration time course for four consecutive puffs at a single sensor.

where $h[n]$ is the *impulse response* of the system. Equation (2) is a standard additive noise communication channel model. However, we have also seen experimentally that the response to a chemical puff varies from puff to puff stochastically as illustrated in FIGURE 3. It is worth noting that the responses shown in FIGURE 3 are for successive puffs (i.e., not distant in time). Thus, unlike typical communication channels, the channel variation is rapid compared to the symbol rate. Furthermore, not only does the amplitude of the response vary, but the very shape of the response varies.

To model such a system, we rewrite equation (2) as

$$Y[n] = \sum_k x[k]H[n-k] + W[n] \quad (3)$$

where $H[n]$ is a *stochastic process* impulse response, $W[n]$ is the sensor noise process and $Y[n]$ is the sensor output process (hence the use of upper case variables). That is, $H[n]$ is a stochastic process that we must characterize through observation of $Y[n]$ under assumptions about $W[n]$.

To determine these characteristics, we sounded the channel with brief chemical pulses (2ms "puffs" – denoted as "1"s) and recorded the time course of concentration at each downstream sensor to obtain a vector of concentration samples, \mathbf{Y} , as in equation (3). Care was taken to adjust the repetition rate and wind speed so that prior puffs did not affect subsequent puff responses. These individual vectors were concatenated to form an observation vector \mathbf{U}_ℓ of dimension $K = N_s M$ where N_s is the number of sensors, M is the number of samples from each sensor and ℓ is the puff index. Defining \mathcal{H}_1 as the puff-present event, the ensemble of responses to L puffs, $\{\mathbf{U}_\ell\}$, $\ell = 1, 2, \dots, L$ was used to determine a sample mean vector

$$\boldsymbol{\mu}_{\mathbf{U}|\mathcal{H}_1} = \frac{1}{L} \sum_{\ell=1}^L \mathbf{U}_\ell \quad (4)$$

and a sample covariance matrix

$$\mathbf{K}_{\mathbf{U}|\mathcal{H}_1} = \frac{1}{L} \left(\sum_{\ell=1}^L \mathbf{U}_\ell \mathbf{U}_\ell^\top \right) - \boldsymbol{\mu}_{\mathbf{U}|\mathcal{H}_1} \boldsymbol{\mu}_{\mathbf{U}|\mathcal{H}_1}^\top \quad (5)$$

for large L .

For simplicity, we assume each of the \mathbf{U}_ℓ is a jointly-Gaussian vector – a not too unreasonable assumption owing to the turbulent

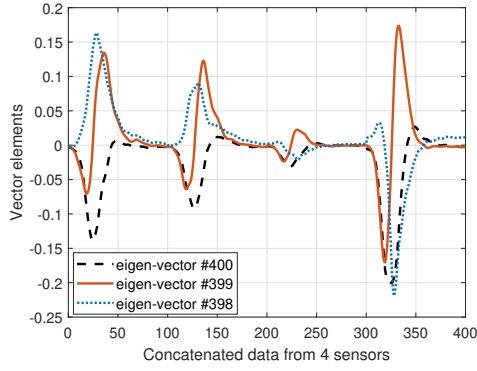


Fig. 4. The three largest- λ principal components of \mathbf{V} for concatenated sensor response \mathbf{U} as described in the text. The symbol rate is 10 bps.

flow structure and the response at a given point is effectively the sum of many random variables. As such we then sought to derive a suitable vector space onto which we could project the \mathbf{U} measurements that would result in mutually independent (or at least uncorrelated in the general case) random variables. Thus, we performed a Karhunen-Loeve expansion [8]–[10] on the covariance matrix $\mathbf{K}_{\mathbf{U}|\mathcal{H}_1}$ to obtain an orthonormal eigenvector matrix \mathbf{V} and diagonal matrix $\mathbf{\Lambda}$ which contains the associated eigenvalues, $\{\lambda_k\}$. That is

$$\mathbf{K}_{\mathbf{U}|\mathcal{H}_1} = \mathbf{V}\mathbf{\Lambda}\mathbf{V}^\top.$$

It is worth noting that \mathbf{V} and $\mathbf{\Lambda}$ mainly capture the random nature of the pulse height and shape induced, ostensibly, by turbulent flow. That is, \mathbf{V} characterizes $H[n]$ not $W[n]$ (which is relatively small compared to the response pulses as shown in FIGURE 3).

\mathbf{V} can then be used to produce a new vector of uncorrelated random variables. The columns of \mathbf{V} represent the basis for dimensions of Karhunen-Loeve expansion. In FIGURE 4, we illustrate a few columns of \mathbf{V} . In this case, \mathbf{V} is generated from the concatenated impulse responses of $N_s = 4$ sensors.

$$\mathbf{Z} = \mathbf{V}^\top \mathbf{U} \quad (6)$$

with mean $\boldsymbol{\mu}_{\mathbf{Z}|\mathcal{H}_1} = \mathbf{V}^\top \boldsymbol{\mu}_{\mathbf{U}|\mathcal{H}_1}$ and covariance $\mathbf{K}_{\mathbf{Z}|\mathcal{H}_1} = \mathbf{\Lambda}$.

We then have

$$f_{\mathbf{U}|\mathcal{H}_1}(\mathbf{u}|\mathcal{H}_1) = \frac{e^{-\frac{1}{2}(\mathbf{u}-\boldsymbol{\mu}_{\mathbf{U}|\mathcal{H}_1})^\top \mathbf{K}_{\mathbf{U}|\mathcal{H}_1}^{-1}(\mathbf{u}-\boldsymbol{\mu}_{\mathbf{U}|\mathcal{H}_1})}}{|2\pi\mathbf{K}_{\mathbf{U}|\mathcal{H}_1}|^{1/2}}$$

which implies that given \mathcal{H}_1 ,

$$f_{Z_i|\mathcal{H}_1}(z_i|\mathcal{H}_1) = \frac{1}{\sqrt{2\pi\lambda_i^2}} e^{-\frac{(z_i-\mu_{Z_i|\mathcal{H}_1})^2}{2\lambda_i^2}} \quad (7)$$

where $\mu_{Z_i|\mathcal{H}_1}$ is the i^{th} component of the mean vector $\boldsymbol{\mu}_{\mathbf{Z}|\mathcal{H}_1} = \mathbf{V}^\top \boldsymbol{\mu}_{\mathbf{U}|\mathcal{H}_1}$.

Similarly, if we denote the no puff event as \mathcal{H}_0 and derive an empirical mean vector $\boldsymbol{\mu}_{\mathbf{S}|\mathcal{H}_0}$ and covariance matrix $\mathbf{K}_{\mathbf{U}|\mathcal{H}_0}$, we have

$$f_{\mathbf{Z}|\mathcal{H}_0}(\mathbf{z}|\mathcal{H}_0) = \frac{e^{-\frac{1}{2}(\mathbf{z}-\boldsymbol{\mu}_{\mathbf{Z}|\mathcal{H}_0})^\top (\mathbf{V}^\top \mathbf{K}_{\mathbf{U}|\mathcal{H}_0} \mathbf{V})^{-1}(\mathbf{z}-\boldsymbol{\mu}_{\mathbf{Z}|\mathcal{H}_0})}}{|2\pi\mathbf{V}^\top \mathbf{K}_{\mathbf{U}|\mathcal{H}_0} \mathbf{V}|^{1/2}} \quad (8)$$

where $\boldsymbol{\mu}_{\mathbf{Z}|\mathcal{H}_0} = \mathbf{V}^\top \boldsymbol{\mu}_{\mathbf{U}|\mathcal{H}_0}$.

Assuming equiprobable \mathcal{H}_1 and \mathcal{H}_0 we can then use the conditional densities on \mathbf{Z} to derive a likelihood ratio test for minimum probability of error as

$$\frac{f_{\mathbf{Z}|\mathcal{H}_1}(\mathbf{z}|\mathcal{H}_1)}{f_{\mathbf{Z}|\mathcal{H}_0}(\mathbf{z}|\mathcal{H}_0)} \underset{\mathcal{H}_0}{\overset{\mathcal{H}_1}{>}} 1 \quad (9)$$

which becomes

$$\frac{\prod_{i=1}^N \frac{1}{\sqrt{2\pi\lambda_i}} e^{-\frac{(z_i-\mu_{1i})^2}{2\lambda_i}}}{|2\pi\mathbf{V}^\top \mathbf{K}_{\mathbf{U}|\mathcal{H}_0} \mathbf{V}|^{-\frac{1}{2}} e^{-\frac{1}{2}(\mathbf{z}-\boldsymbol{\mu}_0)^\top (\mathbf{V}^\top \mathbf{K}_{\mathbf{U}|\mathcal{H}_0} \mathbf{V})^{-1}(\mathbf{z}-\boldsymbol{\mu}_0)}} \underset{\mathcal{H}_0}{\overset{\mathcal{H}_1}{>}} 1 \quad (10)$$

which can be simplified to

$$T(\mathbf{z}) \underset{\mathcal{H}_0}{\overset{\mathcal{H}_1}{>}} \gamma \quad (11)$$

where the test statistic, $T(\mathbf{z})$, is

$$T(\mathbf{z}) = (\mathbf{z} - \boldsymbol{\mu}_0)^\top (\mathbf{V}^\top \mathbf{K}_{\mathbf{U}|\mathcal{H}_0} \mathbf{V})^{-1} (\mathbf{z} - \boldsymbol{\mu}_0) - \sum_{i=1}^N \frac{(z_i - \mu_{1i})^2}{\lambda_i} \quad (12)$$

and the threshold, γ , is

$$\gamma = \left(\sum_{i=1}^N \ln \lambda_i \right) - \ln |\mathbf{V}^\top \mathbf{K}_{\mathbf{U}|\mathcal{H}_0} \mathbf{V}| \quad (13)$$

C. Choosing the Best Dimensions

We note that, N , the dimension of the $\mathbf{K}_{\mathbf{Z}|\mathcal{H}_1}$, can be large and that many of the eigenvalues λ_i may be small relative to the noise in that dimension. For this reason, we seek to use only the “best” D dimensions for our decision rule. However, owing to the experimentally observed fact that the noise process $W[n]$ is not itself white, the largest eigenvalue dimensions of the Karhunen-Loeve expansion for the channel response $H[n]$ may not actually provide the best performance.

While we could ostensibly formulate this as an optimal expurgation problem, we instead ask a simpler question. Suppose we could use only one dimension to make our decision. How would we choose? A simple answer is to employ a heuristic: first, we compose the likelihood ratio test for each dimension (in terms of the parameters μ_{0i} , μ_{1i} , σ_i^2 and λ_i where μ_{0i} and σ_i^2 are the mean and variance, respectively, of Z_i when no puff is presented (\mathcal{H}_0)), and then we calculate the associated probability of error.

Experimental observations suggest that to a first approximation the Z_i are normally distributed under both \mathcal{H}_0 and \mathcal{H}_1 . So, the univariate likelihood ratio is simply

$$\frac{\frac{1}{\sqrt{2\pi\lambda_i}} e^{-(z-\mu_{1i})^2/2\lambda_i}}{\frac{1}{\sqrt{2\pi\sigma_i^2}} e^{-(z-\mu_{0i})^2/2\sigma_i^2}} \underset{\mathcal{H}_0}{\overset{\mathcal{H}_1}{>}} 1 \quad (14)$$

If we shift z left by μ_{0i} and then normalize by $\sqrt{\lambda_i}$, we can naturally define $\mu = \mu_{1i} - \mu_{0i}$ and $\sigma^2 = \lambda_i/\sigma_i^2$ so that equation

(14) becomes

$$\frac{\frac{1}{\sqrt{2\pi\sigma^2}} \exp\left\{-\frac{(z-\mu)^2}{2\sigma^2}\right\}}{\frac{1}{\sqrt{2\pi}} \exp\left\{-\frac{z^2}{2}\right\}} \begin{matrix} \mathcal{H}_1 \\ > \\ \mathcal{H}_0 \end{matrix} > 1 \quad (15)$$

The decision regions for equation (15) are illustrated in FIGURE 5 for $\sigma = 2$ and $\mu = 1$. Equation (15) reduces to

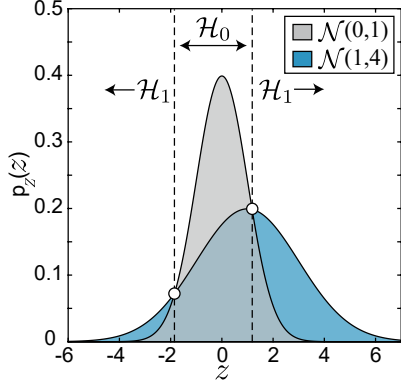


Fig. 5. Decision region illustration for equation (15) for $\mu = 1$ and $\sigma = 2$.

$$\frac{z^2}{2} - \frac{(z-\mu)^2}{2\sigma^2} \begin{matrix} \mathcal{H}_1 \\ > \\ \mathcal{H}_0 \end{matrix} > \ln(\sigma). \quad (16)$$

Then, assuming $\sigma \geq 1$ and defining $\eta = \frac{\mu}{\sigma^2-1}$ and $\zeta = \frac{\mu^2+2\sigma^2 \ln(\sigma)}{\sigma^2-1}$, we can rewrite equation (16) as

$$z^2 + 2\eta z - \zeta \begin{matrix} \mathcal{H}_1 \\ > \\ \mathcal{H}_0 \end{matrix} > 0 \quad (17)$$

We note that while $\sigma < 1$ is possible, it would imply that noise power dominates signal power for that dimension. Thus, we ignore dimensions where $\sigma < 1$ in what follows. In addition, since our covariance estimation window is limited to 800 samples, we will also restrict our selection to dimensions with significant signal power (\approx maximum/1000).

Simplifying the inequality of equation (17) results in the decision regions

$$\hat{\mathcal{H}}_0 : -\eta - \sqrt{\eta^2 + \zeta} \leq z \leq -\eta + \sqrt{\eta^2 + \zeta} \quad (18)$$

which is a symmetric interval of size $2\sqrt{\eta^2 + \zeta}$ centered at $-\eta$, and

$$\hat{\mathcal{H}}_1 : z > -\eta + \sqrt{\eta^2 + \zeta} \text{ or } z < -\eta - \sqrt{\eta^2 + \zeta} \quad (19)$$

The probability of error is

$$P_e = \text{Prob}(\text{say } \mathcal{H}_1 | \mathcal{H}_0) \text{Prob}(\mathcal{H}_0) + \text{Prob}(\text{say } \mathcal{H}_0 | \mathcal{H}_1) \text{Prob}(\mathcal{H}_1) \quad (20)$$

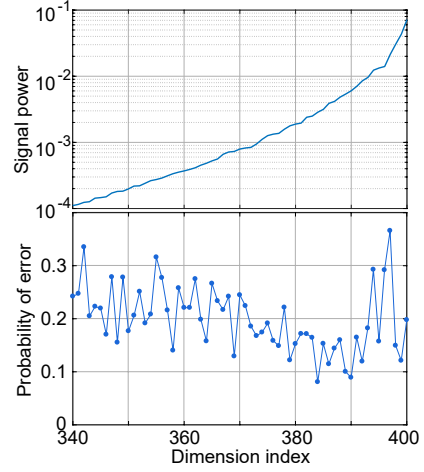


Fig. 6. Probability of error and signal power vs. dimension index for 10 bps data. Larger dimension index implies larger associated eigenvalue.

Then, assuming equiprobable \mathcal{H}_1 and \mathcal{H}_0 , the probability of error is given by

$$P_e = \frac{1}{2} \text{Prob}\left(Z > -\eta + \sqrt{\eta^2 + \zeta} \mid \mathcal{H}_0\right) + \frac{1}{2} \text{Prob}\left(Z < -\eta - \sqrt{\eta^2 + \zeta} \mid \mathcal{H}_0\right) + \frac{1}{2} \text{Prob}\left(-\eta - \sqrt{\eta^2 + \zeta} \leq Z \leq -\eta + \sqrt{\eta^2 + \zeta} \mid \mathcal{H}_1\right) \quad (21)$$

which reduces to

$$P_e = \frac{1}{2} Q\left(-\eta + \sqrt{\eta^2 + \zeta}\right) + \frac{1}{2} Q\left(\eta + \sqrt{\eta^2 + \zeta}\right) + \frac{1}{2} Q\left(\frac{-\eta - \sqrt{\eta^2 + \zeta} - \mu}{\sigma}\right) - \frac{1}{2} Q\left(\frac{-\eta + \sqrt{\eta^2 + \zeta} - \mu}{\sigma}\right) \quad (22)$$

Equation (22) allows us to rank the dimensions of \mathbf{z} according to their individual probability of error performance in terms of μ_{0i} , μ_{1i} , σ_i^2 and λ_i . We plot P_e in FIGURE 6 for dimensions with signal power larger than ≈ 0.001 the maximum. The eigenvalues, ordered from largest to smallest in terms of signal power, are also shown in FIGURE 6. Of course, the analysis leading to equation (22) does not tell us which *ensemble* of D dimensions is the best expurgated version of equation (13). However as a first approximation, sequential application of the equation (22) metric seems reasonable and yields good performance.

D. A Simple Experiment

To test the method, 4 sensors were placed at the tube outlet (1.4m from the emission source) and the resulting responses were recorded for bit rates of 10, 20 and 30 bps. The training set consisted of 800 bits from which $\mathbf{K}_{U|\mathcal{H}_0}$ and thence \mathbf{V} were derived. The D best dimensions were selected according to equation (22). It should be noted that we searched across a number of dimensions. For larger D , performance suffered owing to the inclusion of noisier dimensions. For smaller D , performance suffered from less available signal energy. Typically, the optimal D was in the range $5 \leq D \leq 20$. Once the proper number of dimensions and associated thresholds were established by training, we then applied the resulting detection method to the full data set.

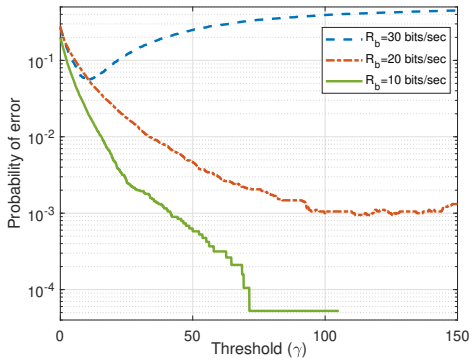


Fig. 7. Probability of error vs. Threshold (γ) for 10, 20 and 30 bps full data sets.

FIGURE 7 shows the probability of bit error rate for the full data set as a function of threshold level γ . We see that P_e is robust with respect to the choice of γ for 10 and 20 bps. So, it is unsurprising that when the threshold calculated using training data is applied to the full data set, we achieved similarly low P_e . At 10 bps, the channel responses do not overlap and there were no errors over 19000 test bits. At 20 bps, P_e was 0.0011, also over 19000 test bits (compared to the minimum from FIGURE 7 of 0.0009). At 30 bps, P_e rose to 0.056 (over 4000 bit intervals) owing to increasing intersymbol interference (ISI). In the next section we consider methods through which ISI can be mitigated.

IV. INTERSYMBOL INTERFERENCE

Higher symbol rates produce ISI which could potentially be mitigated through equalization and/or decision feedback methods [11]. Although we pursue neither such method here, it is worth providing an analytic framework for ISI that takes into account the somewhat peculiar stochastic nature of this channel. Thus, consider an extension of equation (2) to

$$Y[n] = \sum_{i=M}^M b_{-i}H[n - Ni] + W[n] \text{ for } n = 0, \dots, N - 1 \quad (23)$$

where N is the duration of the stochastic impulse response $H[n]$ and $2M$ is the number of incursions, fore and aft, on the 0th bit interval.

Then consider the simplest case of equation (23) where $M = 1$ so the b_0 bit interval is corrupted by both b_{-1} and b_1 . As is typical for ISI/equalization problems, we assume some decision process has provided correct decoding of the prior bit, b_{-1} , and we must formulate a decision rule for the current bit, b_0 , essentially ignoring the interference contribution of the following bit, b_1 . To this end, we measure the channel response covariance conditioned on two priors: $\text{cov}(\mathbf{Y}|b_0 = 1, b_{-1} = 0)$ and $\text{cov}(\mathbf{Y}|b_0 = 1, b_{-1} = 1)$ to obtain two eigenspaces V_0 and V_1 , respectively from which we form $\mathbf{z}_i = V_i^T \mathbf{Y}$ for $i = 0, 1$. Assuming equiprobable bits, the likelihood ratio test when $b_{-1} = i$ is given as

$$\frac{p(\mathbf{z}_i|b_0 = 1, b_{-1} = i, b_1 = 0) + p(\mathbf{z}_i|b_0 = 1, b_{-1} = i, b_1 = 1)}{p(\mathbf{z}_i|b_0 = 0, b_{-1} = i, b_1 = 0) + p(\mathbf{z}_i|b_0 = 0, b_{-1} = i, b_1 = 1)} \underset{\mathcal{H}_0}{\overset{\mathcal{H}_1}{>}} 1. \quad (24)$$

and we apply the appropriate decision rule based on our decision about b_{-1} . Using an *ad hoc* method to obtain “good dimensions” similar to equation (22), P_e dropped from 0.056 to 0.030, and we were able to achieve a $P_e = 0.15$ at 40 bps. Note that at 40 bps, each bit interval is corrupted by roughly four adjacent bits (two fore and two aft), so “equalization” methods that accounted for more than one bit of ISI could improve performance.

V. CONCLUSION

We measured the output of multiple PID sensors in response to a chemical puff emitted within a meter-scale channel at constant velocity gas flow. The response between input and output was found to be stochastic due to unsteady flow, but was shown (on average) to be linear. The channel description was formalized and an appropriate signal space derived from signal covariance estimates. Using a simple likelihood ratio test, a data rate of 10 bps was achieved without errors. Increased data rate led to ISI and thus increased error rate (10^{-3} at 20 bps, 0.056 at 30 bps). We then framed the ISI problem more carefully and using rudimentary methods were able to achieve a P_e of 0.15 at 40 bps and reduce P_e to 0.03 for 30 bps. As much of the previous molecular/chemical communications literature deals with diffusive transport mechanisms where accurate bit rates are less than 1 bps, this work improves the prospects for fast embedded molecular communication in both medical, device and industry applications by approximately two orders of magnitude.

ACKNOWLEDGMENT

This research was supported by funding from the Defense Advanced Research Projects Agency (DARPA). The views, opinions and/or findings expressed are those of the author and should not be interpreted as representing the official views or policies of the Department of Defense or the U.S. Government. This work was also supported in part by a Brown University Research Seed Award.

REFERENCES

- [1] N. Farsad, W. Guo, and A.W. Eckford. Tabletop Molecular Communication: Text Messages through Chemical Signals. *PLOS ONE*, 8(12):e82935, 2013.
- [2] S. Ghavami, R. Adve, and F. Lahouti. Bounds on the capacity of ASK molecular communication channels with ISI. In *2015 IEEE Global Communications Conference*, 2015.
- [3] C. Rose and I. S. Mian. Inscribed Matter Communication: Part I. *IEEE Transactions on Molecular, Biological and Multi-Scale Communications*, 2(2):209–227, Dec 2016.
- [4] C. Rose and I. S. Mian. Inscribed Matter Communication: Part II. *IEEE Transactions on Molecular, Biological and Multi-Scale Communications*, 2(2):228–239, Dec 2016.
- [5] N. Farsad, D. Pan, and A. J. Goldsmith. A Novel Experimental Platform for In-Vessel Multi-Chemical Molecular Communications. *CoRR*, vol. abs/1704.04810, 2017.
- [6] K. V. Srinivas, A. W. Eckford, and R. S. Adve. Molecular communication in fluid media: The additive inverse gaussian noise channel. *IEEE Transactions on Information Theory*, 58(7):4678–4692, 2012.
- [7] P. Shakya, E. Kennedy, C. Rose, and J. K. Rosenstein. Correlated Transmission and Detection of Concentration-Modulated Chemical Vapor Plumes. *IEEE Sensors Journal*, 2018. submitted (in review).
- [8] M. Loève. *Probability Theory*. D. Van Nostrand Company Inc., 1960.
- [9] H.L. Van Trees. *Detection, Estimation, and Modulation Theory, Part I*. Wiley, New York, 1968.
- [10] J.M. Wozencraft and I.M Jacobs. *Principles of Communication Engineering*. Wiley, 1965.
- [11] J.G. Proakis and M. Salehi. *Digital Communications*. McGraw-Hill International Edition. McGraw-Hill, 2008.